Acoustic Doppler Current Profiler Measurements from Saildrones, with Applications to Submesoscale Studies

Paban Bhuyan,[a] Cesar B. Rocha,[b] Leonel Romero,[a] and J. Thomas Farrar [c]

[a] *University of Connecticut, Avery Point, CT, USA*

[b] *University of São Paulo, São Paulo, SP, Brazil*

[c] *Woods Hole Oceanographic Institution, Woods Hole, MA, USA*

Corresponding author: Paban Bhuyan, paban.bhuyan@uconn.edu

ABSTRACT: Characterizing submesoscale ocean processes requires high-resolution observations in both space O(1 km) and time O(1 hr). One way to resolve submesoscale features is to deploy multiple mobile platforms, such as Saildrones (SDs), to achieve high-resolution synchronous measurements, but this requires velocity accuracies of O(1 cm/s) to resolve submesoscale velocity gradients. In this study, we first assess Saildrone Acoustic Doppler Current Profiler (ADCP) measurements against a high-quality shipboard (R/V *Oceanus*) ADCP data, both collected during the Sub-Mesoscale Ocean Dynamics Experiment (S-MODE). The results show that the standard 5-minute average Saildrone ADCP along-track velocity difference variability (3 cm/s) is consistent with shipboard ADCP data, confirming its suitability for submesoscale studies. However, direct ADCP comparisons between a Saildrone and the R/V *Oceanus* give small biases (~1 cm/s). The biases are unlikely due to the surface waves, whose signal is expected to be significant near the surface; they are more likely be associated with spatial inhomogeneities. We also examined the 1 Hz Saildrone ADCP data to determine the best averaging window for high-resolution analyses and found that averaging over 3 minutes (~250 m in space) reduces the noise to acceptable levels. We investigate the uncertainty of submesoscale current gradients derived from Saildrone ADCP measurements and find that the velocity gradient at a 2 km scale can be obtained with a $0.1f$ uncertainty using four Saildrones. The methodologies we developed to ascertain optimal averaging window are versatile and applicable to other uncrewed surface vehicles (USV) or multiple-ship arrays.

SIGNIFICANCE STATEMENT: Submesoscale currents, spanning from a few hundred meters to several kilometers and lasting from hours to weeks, play a key role in transferring energy and redistributing water properties, influencing air-sea interactions and shaping marine ecosystems. However, observing these currents is challenging. Saildrone, an innovative platform, collects oceanic and atmospheric data, including ocean currents, but assessing and refining this data is essential for studying submesoscale processes. In this paper, we assess the ocean current measurements from Saildrone and develop methods to characterize noise in the data. We then use this improved data to estimate the uncertainty in the current measurements and their gradients, helping us determine the reliability of the data for analyzing submesoscale flow characteristics.

1. Introduction

Submesoscale currents have emerged as an important component of the upper-ocean circulation. These currents (in the vicinity of submesoscale fronts, filaments and vortices) with horizontal length scales of 0.1-10 km and timescales of hours to days are characterized by order-one Rossby and Richardsons numbers (McWilliams 2016), which makes them dynamically distinct from mesoscale currents (Mahadevan and Tandon 2006). Submesoscale flows exhibit large vertical velocities (up to several cm/s). These large velocities are believed to promote substantial exchanges between the mixed layer and the pycnocline, as well as across the air-sea interface, with significant implications for ocean biogeochemical and heat fluxes, respectively— eventually affecting climate (e.g., Lévy et al. 2012; Su et al. 2018).

Most of our knowledge about submesoscale processes comes from theory and numerical models, and therefore accurate spatio-temporal velocity observations are required for validation. In this context, contemporary simultaneous autonomous observational tools and ship surveys, particularly those utilizing the Acoustic Doppler Current Profiler (ADCP), stand out as apt choices for making these observations. Shipboard current measurements using ADCPs have been a standard for over forty years (Joyce 1989). ADCPs with a 4-beam Janus configuration measure the Doppler frequency shift of the transmitted acoustic pulse, providing estimates of the currents. More recently, autonomous uncrewed surface vehicles such as Saildrones (Zhang et al. 2019; Gentemann et al. 2020) and Wavegliders (Hodges et al. 2023) have been used to measure upper-ocean currents. These platforms will be especially useful for collecting synchronous measurements from multiple platforms in formation to enable the estimation of horizontal velocity gradients. This approach was employed in the Saildrone component of the S-MODE field campaigns, which specifically aimed to collect concurrent velocity measurements at submesoscale resolution using formations of vehicles. In these field campaigns, RDI ADCP-equipped Saildrones, each with 7 m long hull and 5 m tall wing, were deployed in tight formations with approximately 1 km spacing to measure ocean velocities, from which we estimate velocity gradients.

Saildrones are much smaller than most ships, so it is possible that their ADCP measurements could be compromised by winds and waves. Their relatively small size means that Saildrones are more strongly affected by steep short waves and susceptible to rolling and pitching, potentially leading to errors in current calculations. High-frequency ADCP observations on Saildrones are thus subject to numerous potential sources of error and bias. These include instrument noise, the effects of high-frequency surface gravity waves, inaccuracies in positioning, signal quality issues, pitch and roll effects, heading bias, fish schooling bias, and wave-induced drift bias. These errors and biases in absolute velocities can stem from either relative velocity measured by the ADCP or the measured platform velocity and orientation. It is therefore crucial to characterize potential biases and errors in Saildrone ADCP data. Submesoscale processes, with velocity signals that are relatively weak compared to large-scale processes, demand high-accuracy, dense observations. Simple propagation of errors suggests we need a root mean square velocity error of about 1 cm/s to resolve a velocity gradient with an accuracy of O(0.1 f) at a 1 km separation in midlatitudes.

Previous studies have used a "frozen field" approximation when estimating velocity gradients with a small number of platforms, i.e., treating data taken at different times and locations by a moving platform as if the platform moved infinitely fast and the data were taken synoptically. This interpretation of the data may confuse temporal and spatial variability, which is a form of aliasing. For example sampling from a single platform following a radiator pattern (e.g., Rudnick 1996) leads to space-time aliasing, especially at small sacales, which evolve quickly. More recent studies have employed two ships simultaneously (e.g., Shcherbina et al. 2013; Qu et al. 2022) to account for cross-track velocity gradients, but these still rely on the assumption of a frozen field along the ship tracks. It is important to note that when we refer to unaliased (instantaneous) data in our analysis, those data are not truly unaliased, as we perform averaging of the raw data to remove surface wave and noise signals, which inherently introduces a different form of aliasing. This aliasing results from the smoothing out of high-frequency variability.

Our primary objective is to quantify the uncertainties of salidrone ADCP velocities and their gradients computed from two or more platforms. We first quantify biases in the velocity data by comparing them against high-quality ship-based ADCP observations. Then, we examine the noise and unwanted wave signals in velocity data through spectral analysis, velocity difference variability, and structure functions. These analyses are used to consider the temporal and spatial averaging windows that are appropriate to achieve high-resolution and high-quality velocity data for submesoscale studies. Further, the high-quality velocity data are used to estimate horizontal velocity gradients through least-squares plane fits.

The paper is organized as follows: Section 2 describes the S-MODE Field campaign, including the environmental conditions of the region, sampling strategies, and instrumentation. Section 3 details the methodology adopted, and Section 4 presents the results, which include Saildrone ADCP data validation against ship-based ADCP observations, an analysis of optimal averaging to reduce uncertainties, and a characterization of the uncertainties of the derived velocity gradients. Finally, Section 5 summarizes our findings.

2. Field campaign

The data used in this study were collected as part of the Sub-Mesoscale Ocean Dynamics Experiment (S-MODE), a NASA-funded project with the main goal of exploring the role of submesoscale vertical transport in the upper ocean. S-MODE brought about a significant advancement in the observational capabilities of submesoscale processes. The experiment employed a range of observational tools, including aircraft-based remote sensing, satellite remote sensing, ship-based measurements, drifter deployments, and a fleet of autonomous vehicles (including Saildrones). The observational phase of S-MODE encompassed three field campaigns, all carried out in the northeast Pacific Ocean within a region influenced by the California Current System approximately 100 km off the coast of San Francisco Bay. We deployed arrays of Saildrones in two of the S-MODE field campaigns (Figure 1a and b). The Pilot campaign was conducted in 2021 (October 19 to November 6) and the first Intensive Operations Period (IOP-1) in 2022 (October 3 to November 7). In this study, we analyze data collected during both campaigns.

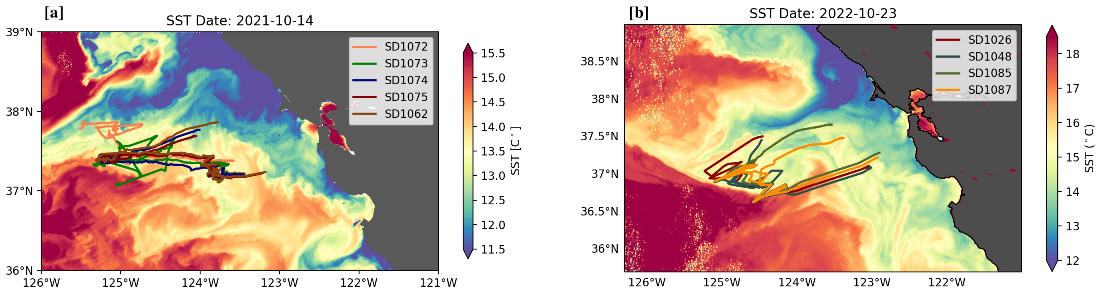

FIG. 1. Map of the study region off central California showing the representative sea surface temperature (colors) measured by satellite (VIIRS - Visible Infrared Imaging Radiometer Suite) during the Pilot Campaign [a] and IOP-1 [b] campaigns. The solid lines show the Saildrone tracks during each respective field campaign which are not necessarily coincident in time with the VIIRS data.

a. Oceanographic conditions

The California Current System (CCS) is an intricate network of large-scale currents and water masses. It comprises various large-scale currents such as the California Current, California Under Current (CUC), Davidson Current, and the spring/summer equatorward coastal current. It includes diverse water masses such as the Pacific Subarctic Water, North Pacific Central Water, and CUC Southern Water, which are influenced by river outflows (e.g., Marchesiello et al. 2003). The CCS is among the most studied major eastern boundary upwelling systems worldwide (Kämpf and Chapman 2016). In the CCS, cold water upwelled particularly near canyons, creates surface density gradients that sustain mesoscale eddies and filaments, transporting these features hundreds of kilometers offshore into the oligotrophic region (Kessouri et al. 2020). The sharp horizontal density gradients release available potential energy, supporting the generation of submesoscale processes in the surface layer (Capet et al. 2008; McWilliams 2016). The S-MODE research focuses on these submesoscale features, targeting high-resolution in-situ velocity observations using ADCPs mounted on several different platforms. Figure 1 illustrates the general SST pattern near the S-MODE site, which is qualitatively similar during the two field campaigns, where wind speeds reached up to 15 m/s and significant wave heights reached 9 m during the Pilot and 4.5 m during IOP-1.

b. Instrumentation

The Saildrones were each equipped with a downward-looking 300 kHz R. D. Instruments ADCP, sampling at 1 Hz, and an inertial navigation system (VectorNav VN-300), sampling at 20 Hz. The VN300 measures vehicle position, heading, pitch, roll and heave, and these data are used to convert the ADCP relative velocities into absolute velocities in earth reference frame. The ADCP was mounted on the keel, at a depth of 1.9 m below the waterline. The transducers transmit pulses every second, each lasting for a few milliseconds. The Doppler shift in the returned signal is measured for each beam and mapped onto 50 range 2-m vertical bins. The first velocity measurement is at 6 m because a 4-m blanking distance is set to avoid acoustic artifacts very close to the acoustic transducers.

c. Sampling strategy

Arrays of Saildrones was deployed during each campaign, five during the Pilot (SD1062, SD1072, SD1073, SD1074, and SD1075) and four during IOP-1 (SD1026, SD1048, SD1085, and SD1087), with the goal of measuring velocity gradients at kilometer scales across fronts, filaments, and instabilities (Figure 1). In this study, we analyze data from two sampling modes: the inter-platform configuration during the Pilot (Figure 2a) and quadrilateral formation using four Saildrones during IOP-I (Figure 9). The inter-platform leg comparison involved two Saildrones and the R/V *Oceanus* sailing parallel tracks separated by less than 2 km for 9 hours, with Saildrone SD1072 positioned closer to the ship (Figure 2a). During the quadrilateral formation (henceforth quad formation), four Saildrones moved synchronously across a front, maintaining a spacing of approximately 1 km. Navigating an array of Saildrones in tight formation can be challenging, particularly in adverse wind and wave conditions and across strong currents. Despite these challenges, we were able to maintain the quad formation without significant distortions for 36 hours from 19 October 2022 to 21 October 2022.

3. Methods

a. Standard Processing

ADCP measurements are subject to several sources of errors that can affect the accuracy of the derived absolute velocity. Here we describe the processing steps involved in obtaining the velocity from the Saildrone ADCP. The process of deriving absolute velocity from relative velocity and vehicle velocity involves several steps, namely (i) the conversion of measured Doppler shift in the returned signal by the scatterers to beam velocity, (ii) beam velocity transformation to instrument coordinates, (iii) transformation of velocities from instrument coordinates to platform coordinates, and (iv) transformation of platform coordinates to Earth coordinates. The final estimated velocity reflects the ocean currents. The ADCP has four transducers aligned in the bow, aft, port, and starboard directions of the Janus configuration, each tilted 20° from the platform's center line, providing one redundant beam. The redundant information improves the confidence in the measurements by providing error-velocity estimates. In the case when one of the beams has bad data, this redundant beam helps measure velocities using the three-beam solution. The screening algorithm marks bad bin data for a particular beam bin if the percent good for that given beam at that depth is 0 (Teledyne 2010).

Motion contamination on ADCP velocities occurs due to translation velocity of the ADCP, angular velocity of the ADCP from platform rotation and tilt caused by pitch, roll, and heading variations. Motion correction is performed using the attitude angle, angular velocity, and translation velocity obtained from the VN-300 IMU mounted on the Saildrone. The range-gated ADCP bins are not vertically oriented during pitching and rolling motion, and the bins for each beam are remapped using pitch/roll angle to the nearest 2-m vertical bin without any smoothing or interpolation.

The CPU onboard Saildrone performs ping-by-ping corrections for tilt, velocity, angular velocity, speed of sound, bad beam velocity, heading misalignment, etc. This includes using the near-surface hydrographic data from a conductivity-temperature-depth probe to correct for variations in sound speed. All screening, calibration, and processing steps are also performed onboard, including the specific step of deriving velocity in Earth coordinates from the Doppler shift measured for each beam, before the distribution of the data. After the remapping and other corrections are performed onboard the Saildrone CPU, the 1 Hz processed data written to the disk onboard the Saildrone are averaged with a window length of 5 minutes to reduce the impacts of wave motion, GPS vertical-axis errors, and pitching motion. These average data are then transmitted via satellite in near-real-time to Saildrone Inc. headquarters, while 1 Hz raw data are saved to disk onboard and retrieved after the Saildrones are recovered.

b. Heading Misalignment Calibration

The errors in the heading can introduce large uncertainties for current measurements with ADCP (Kosro 1985; Alderson and Cunningham 1999). Therefore heading misalignment calibration between the platform and the ADCP beams is a common check performed on most platforms mounted ADCPs. For this, bottom tracking was activated for the Saildrones in shallow water (<500 m) over the shelf on their way to the sampling region and their return to San Francisco Bay. During bottom tracking mode, transducers emit a long pulse (ping) between a set of normal pulses and measure the Doppler shift in the signal reflected from the ocean floor. This is the bottom (ocean floor) velocity relative to the ADCP (i.e., the opposite of platform velocity measured by IMU/GPS). The number of hours of bottom tracking data, along with the misalignment angles, is detailed in Table 1. The misalignment angle is calculated by evaluating the phase difference between the bottom-tracking vehicle velocity and the vehicle velocity obtained from the GPS/IMU using a cross-correlation method. Additionally, the method for water velocity calculation that uses both the misalignment angle and an adjustment factor for scaling of Doppler current to remove overall system bias (Joyce 1989) yielded similar misalignment angles (as in Table 1) and an amplitude correction under 1%, which was deemed negligible and thus omitted.

Heading misalignment correction is important, as any small misalignment (θ) in along-track direction can add a velocity error to the cross-vehicle velocity equal to $\sin\theta$ times the vehicle speed. The calculation of heading misalignment using bottom-tracking data, as shown in Table 1, suggests that the error due to misalignment is relatively small, with misalignment angles ranging from 0.13° to 1.65°. For the maximum Saildrone speed of 1.5 m/s, this heading misalignment translates to an error in the range of 0.3–4 cm/s in the athwartship velocity. However, the misalignment angle correction did not significantly affect the mean velocity (Table 1).

c. Velocity difference variability

The standard deviation of the velocity difference for various averaging time windows t was calculated according to

$$\sigma_{\Delta u}(t) = \langle \sqrt{\overline{(\Delta u_t')^2}} \rangle_{n,z} \,, \tag{1}$$

TABLE 1. Analysis of misalignment angle corrections for along- and cross-track velocity component using bottom track (BT) data for Saildrones. BT data duration, represents the bottom track data used for the analysis. The misalignment angle is evaluated from the BT data and the GPS/IMU data as discussed in section 3b. $\overline{\Delta u_{along}}$ represents the mean difference between the corrected and uncorrected along-track velocities, $\overline{\Delta u_{cross}}$ represents the mean difference between the corrected and uncorrected cross-track velocities. NA: Insufficient quality data for misalignment angle analysis.

Saildrone ID	BT Data Duration (hours)	Misalignment Angle (degrees)	$\overline{\Delta u_{along}}$ (m/s)	$\overline{\Delta u_{cross}}$ (m/s)
SD1062	78	0.08	-0.0000	-0.0001
SD1072	77	0.22	-0.0001	-0.0003
SD1073	109	1.49	-0.0006	-0.0019
SD1074	NA	NA	NA	NA
SD1075	NA	NA	NA	NA
SD1026	72	0.64	0.0003	0.0000
SD1048	72	0.50	0.0002	0.0001
SD1085	48	0.56	-0.0001	-0.0003
SD1087	48	0.14	-0.0000	-0.0001

where Δu_t is the velocity difference between data points separated by time t, i.e., $\Delta u_t = u(\tau+t) - u(\tau)$, and $\Delta u'_t = \Delta u_t - \overline{\Delta u_t}$ and $\langle\cdot\rangle_{n,z}$ is the ensemble average over all realizations and depths. Our rationale for choosing velocity difference variability is that it directly informs us about the expected variability at different scales. We also use the velocity difference variability as a metric to compare the current variability at O(1 km) scale of Saildrone and ship-based ADCP measurements.

d. Spectral Analysis (time and space)

For the computation of kinetic energy (KE) spectra in frequency or space domains we selected 36 hours of data from both Pilot and IOP-1 field campaigns. These corresponded to 7 transects of length about 16 km in the Pilot and 4 transects of length about 30 km in IOP-1. We then performed linear interpolation to fill any missing data points within each transect and at every depth, detrended the data, and applied a Hanning tapering window (Romero and Melville 2010; Rocha et al. 2016). Additionally, we adjusted the estimated spectra to compensate for the variance loss caused by tapering. Based on a depth decorrelation analysis, we obtained an average vertical e-folding decorrelation length of 14m corresponding to 7 bins out of 21, which implies nearly three independent realizations per transects. This resulted in 21 realizations for the Pilot and 12 for

IOP-1, leading to 42 and 24 degrees of freedom (DOF), respectively for the depth-average spectrum in Figure 4 and 5. The depth-average velocity difference variability, and structure-function analysis described later also shares the same data and DOF (Figure 6, 7).

e. Structure Functions

The analysis of KE spectra and second-order structure functions have been applied to gain insights into the distribution of energy across different scales (Ferrari and Wunsch 2010; Callies and Ferrari 2013; Poje et al. 2017), but here we use it to find the optimal averaging window of the data for submesoscale studies. To calculate the second-order structure function, we utilized the same transects that were used for the spectral analysis. We interpolated the 1 Hz data to achieve a 1-meter horizontal resolution at all depths for all transects, ensuring evenly spaced data for the structure-function calculation. The structure function values were then calculated at increments of n meters, where n is an array index starting from 1 and increasing to the total number of observations in the 1-meter resolution transect data. The structure function was computed at each depth for all transects and then averaged together resulting in a single representative structure function for each Saildrone.

The structure-function was calculated as

$$S_r = \langle \overline{(\Delta u_r)^2} \rangle_{n,z} , \tag{2}$$

where the velocity difference $\Delta u = u(x+r) - u(x)$, $\overline{(\Delta u_r)^2}$ is the mean velocity-difference-square, which is a function of the scale r (array of n meters), and $\langle \cdot \rangle_{n,z}$ is the ensemble average over all realizations and depths. The second-order structure function exhibits a scaling behavior of $S_r \sim r^{\beta-1}$ for an energy spectrum following a power-law of $E(k) \sim k^{-\beta}$ (e.g., Bennett 1984). Hence, in the case of submesoscale resolving simulations/observations if the KE spectra scales as k^{-2}, the corresponding structure function would scale as r^1 (Choi et al. 2017; Essink et al. 2019).

f. Velocity gradients

Velocity gradients are enhanced at submesoscales and derived kinematic properties such as vertical vorticity, horizontal divergence, and lateral strain rate play a crucial role in submesoscale dynamics (e.g., Shcherbina et al. 2013; D'Asaro et al. 2018). Observing submesoscale velocity gradients in the ocean is challenging as measurements must be collected from at least two ships/platforms (Shcherbina et al. 2013). In this study, we use two or more platforms to calculate submesoscale current gradients by fitting a plane to the available data within a moving window of 2 km by 2 km along the average trajectories of the Saildrones. By applying a least-squares (LS) plane fit to the velocity data within the search box, the velocity gradients can be obtained as coefficients of the fit, under the assumption of a local linear approximation of velocity around a central point (e.g., Okubo and Ebbesmeyer 1976; Molinari and Kirwan 1975; Shcherbina et al. 2013):

$$\mathbf{U} \approx \bar{u} + u_x(\mathbf{x} - x_0) + u_y(\mathbf{y} - y_0) \tag{3}$$

$$\mathbf{V} \approx \bar{v} + v_x(\mathbf{x} - x_0) + v_y(\mathbf{y} - y_0)\,, \tag{4}$$

where $\mathbf{U} = [u_1, u_2, \ldots, u_n]^{\mathrm{T}}$ and $\mathbf{V} = [v_1, v_2, \ldots, v_n]^{\mathrm{T}}$ represent observed velocity vectors, and $\mathbf{x} = [x_1, x_2, \ldots, x_n]^{\mathrm{T}}$ and $\mathbf{y} = [y_1, y_2, \ldots, y_n]^{\mathrm{T}}$ denote the position vectors. On the right, ($\bar{u}$, $\bar{v}$) is the average velocities, (x_0, y_0) is the centroid position of the search window, and u_x, v_x, u_y, and v_y are the velocity gradients. The matrix form of equations (3) and (4) is given by

$$\mathbf{U} \approx \mathbf{X}\mathbf{A_u}, \tag{5}$$

$$\mathbf{V} \approx \mathbf{X}\mathbf{A_v}, \tag{6}$$

with $\mathbf{A_u} = [\bar{u}, u_x, u_y]^{\mathrm{T}}$, $\mathbf{A_v} = [\bar{v}, v_x, v_y]^{\mathrm{T}}$, and

$$\mathbf{X} = \begin{bmatrix} 1 & (x_1 - x_0) & (y_1 - y_0) \\ 1 & (x_2 - x_0) & (y_2 - y_0) \\ \vdots & \vdots & \vdots \\ 1 & (x_n - x_0) & (y_n - y_0) \end{bmatrix}. \tag{7}$$

From the velocity gradients estimated through plane fits, we compute vertical vorticity $\zeta = v_x - u_y$, lateral divergence $\delta = u_x + v_y$, and lateral strain rate $\alpha = [(u_x - v_y)^2 + (v_x + u_y)^2]^{1/2}$.

To account for the Saildrone ADCP data uncertainty, we employ a weighted least-squares (LS) plane fit to determine the velocity gradients. We also estimate the uncertainty of the velocity gradients by propagating the error in the velocities to their gradients. The detailed calculation of the uncertainty in the coefficients is described in Appendix A for the weighted LS fitting. The weighted LS fit takes into account the uncertainties of the currents from each Saildrone, minimizing the uncertainty of the fitted current gradients. Weights are calculated from the standard errors of 1 Hz data averaged to 3 or 5 minutes.

We also considered the aspect ratio of the formation of the data contained within the box, which is important for the accuracy of the velocity gradient estimates. Here the aspect ratio γ is defined as the ratio of the minor eigenvalue (λ_{min}) to the major eigenvalue (λ_{max}), which is estimated from the position covariance matrix $\gamma = \lambda_{min}/\lambda_{max}$ (Choi et al. 2017). Saildrone formations with an aspect ratio value $\gamma < 0.2$ were discarded (Ohlmann et al. 2017), which occurred when Saildrones were drifting with elongated formations.

4. Results

Validating the Saildrone velocity measurements and quantifying its noise are critical steps for using these data for studying submesoscale currents. Once we have a clear grasp of the uncertainty in the velocity measurements, we can better determine the corresponding uncertainty in the velocity gradients and derived kinematic quantities (vertical vorticity, horizontal divergence, and lateral strain rate). This section compares the Saildrone velocity measurements against synchronous ADCP measurements made with an research vessel. This is followed by an analysis of the high-frequency noise to estimate the amount of averaging necessary to attain submesoscale currents with a reasonable noise-to-signal ratio. Finally, the averaged data, with quantified uncertainty, are used to estimate submesoscale velocity gradients and associated uncertainties.

a. Comparison against ship-based observations

During the Pilot field campaign, two Saildrones (SD1072 and SD1073) and the R/V *Oceanus* collected ADCP measurements along parallel tracks for 9 hours. Both Saildrones and the R/V *Oceanus* were equipped with R.D. Instruments Workhorse 300 kHz ADCPs that sampled at 1 Hz, providing a uniform basis for comparison. To minimize the aliasing effect of high-frequency signals, we used 5-minute averaged data when comparing the velocity data of both platforms. Additionally, we limited our analysis to periods when the platforms were located within 2 km from one another. We also restricted the comparison to the top 50 m of the water column, where ADCP instrument noise is less prominent. Saildrone ADCP data were linearly interpolated in depth to the *Oceanus'* ADCP depth bins between 10 m (shallowest *Oceanus* ADCP measurement) and 50 m. We performed three types of comparison: visual (spatial), direct, and statistical.

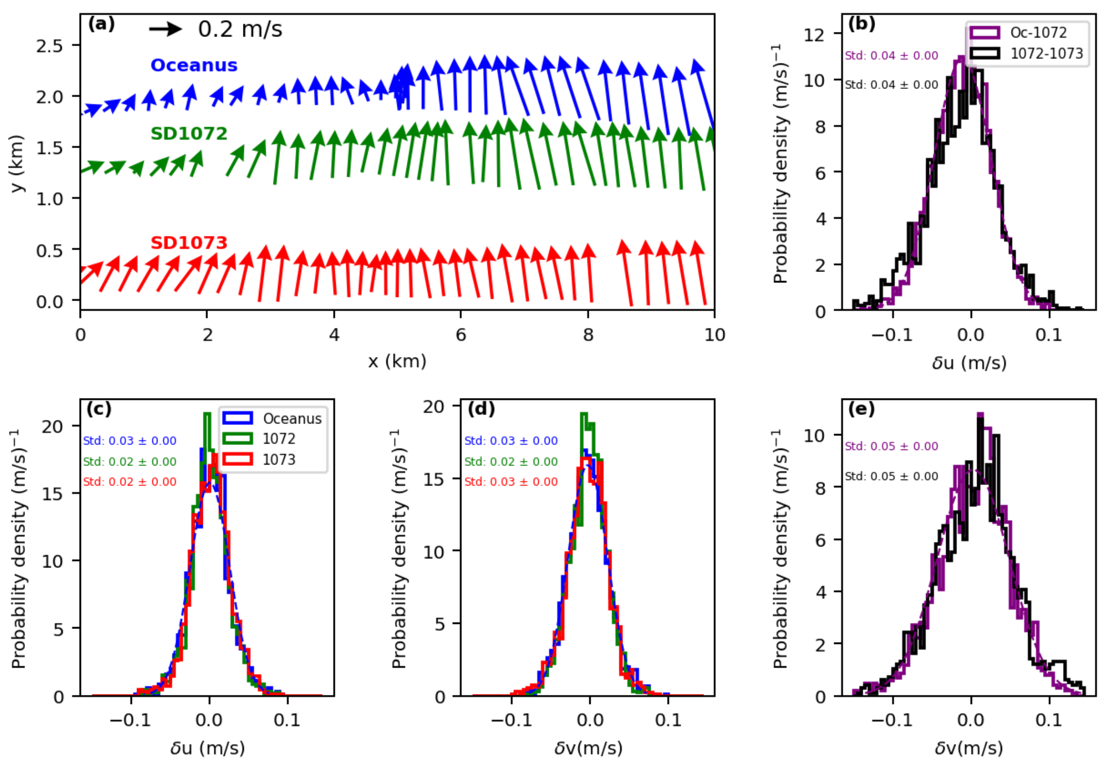

FIG. 2. Comparison of current vectors and velocity differences for R/V *Oceanus* and two Saildrones. (a): Current vectors from R/V *Oceanus* (blue), SD1072 (green), and SD1073 (red) at 10 m depth for a track section where platforms were separated by less than 2 km. PDFs of velocity difference between 10-50 m depths for platform pairs are shown in (b and e), and along each platform in (c and d). Panels (b,c) and (d,e) display the velocity differences for δu and δv, respectively, with standard deviations indicated.

We first compare the velocity vectors at 10 m depth spatially in Figure 2a. The data show visual agreement between the *Oceanus* and the closest Saildrone, with stronger currents on the right of the track and substantial variability at kilometer scale. In contrast, the Saildrone (SD1073) located 2 km from the *Oceanus* shows slightly weaker velocity lateral gradients.

Scatter plots directly comparing the u and v velocities at depths between 10 and 50 m of the nearest Saildrone to the R/V *Oceanus* exhibit a pronounced correlation with a slope of 0.93 for the east-west (u) velocity component and 1.0 for the north-south (v) velocity (Figure 3). The root-mean-square difference for both the u and v is 0.1 m/s. Additionally, there is a net bias of +1 cm/s

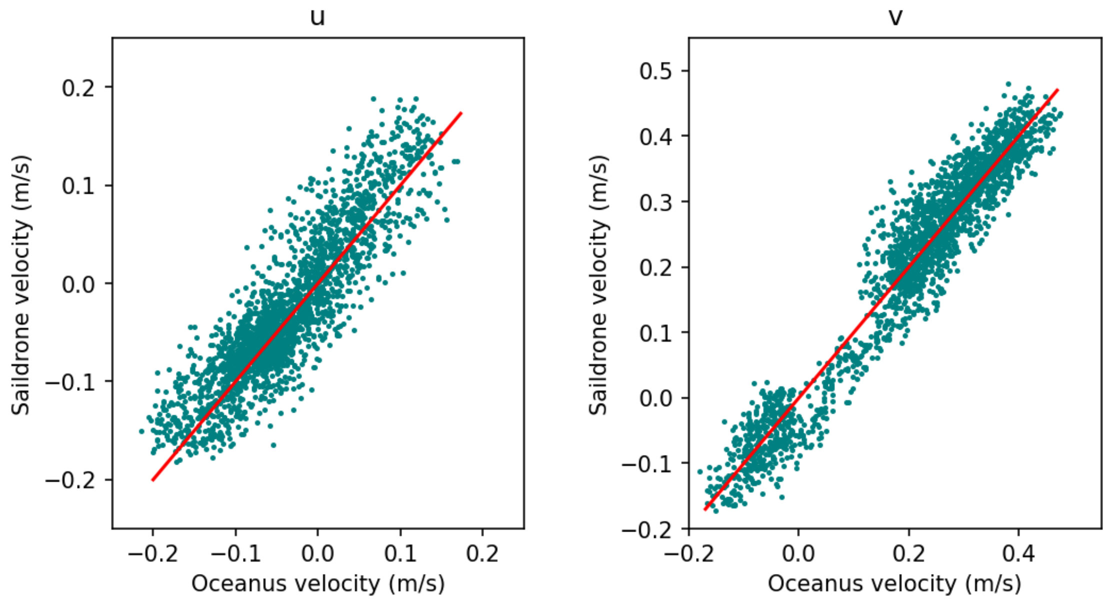

FIG. 3. R/V *Oceanus* and the closest Saildrone (SD1072) scatter plot for u and v velocity components. The red line represents the 1:1 correlation.

in the u component and 0.2 cm/s in the v component. This net difference is likely dominated by the inherent natural variability existing at these separation scales, and is further analyzed as a function of depth in Section 4c.

The statistical comparison between the Saildrone and ship ADCP measurements was carried out in two ways. The first analysis involved comparing the probability density functions (PDFs) of along-track (east-west and north-south) velocity differences. In this analysis we estimated the root-mean-square (rms) velocity-difference variability ($\sigma_{\delta u}$) for each platform from 9 hours of Pilot ADCP data when they were cruising in parallel tracks. The results show that all platforms observed similar velocity-difference variability at this scale (~500 m) separation with $\sigma_{\delta u}$ for both u and v components and all platforms less than 3 cm/s (Figure 2c, 2d). Also, the along-track velocity differences in the IOP-1 Saildrone ADCP 5-minute data (not shown) also give the same velocity difference variability of 3 cm/s at 500 m. To assess the significance of the similarity between the *Oceanus* and Saildrone velocity difference PDFs, each with 2142 observations, we used the Kolmogorov-Sriminov test (Press 1992; Rudnick 2001), which indicates that the samples are 99.98% statistically similar.

The second PDF analysis involves comparing the PDFs of velocity-difference between platform pairs, which shows standard deviations of δu and δv for all platform pairs being $\leq$ 4 cm/s (Figure 2b, 2e). These results suggest that the two platforms give statistically similar results at the scales analyzed. Additionally, the overall correspondence between the Saildrone and the R/V *Oceanus* ADCP profiles was reasonable, with bias of ~1 cm/s. While it is possible that the Saildrone, due to its smaller size, could be more responsive to short, steep waves compared to the ship, we are unable to quantify any wave-related biases. This is because the ship's ADCP measurements start at a depth of 10 m, where wave bias is expected to be minimal (Amador et al. 2017; Hodges et al. 2023). It is important to note that this Saildrone-ship comparison does not provide complete information about the uncertainty of Saildrone ADCP measurements, which we discuss in the next subsection.

b. Temporal and spatial averaging

Measuring currents at a frequency of 1 Hz, the Saildrone ADCP captures substantial high-frequency variability that needs to be minimized before the data can be used in the analysis of submesoscale currents. The frequency spectra shown in Figure 4 exhibit three distinct ranges, which we identify as natural variability with a power-law slope of approximately -2, noise with a flat spectrum, and high-frequency variability due to surface waves. The KE spectra suggest that surface wave signals with periods of 2-15 seconds, which was confirmed by the coherence of pitch and roll with along- and across-platform velocities, respectively. The white noise ranges on average from about 16 to 180 seconds. The cumulative integral of the KE spectrum for the resolved frequencies suggests that the noise band between 16-180 seconds contributes to only a minor fraction of approximately 4% of the total KE, while high-frequency surface wave signals contribute to 76% of the KE. The remaining 20% of KE represents the contribution from submesoscale variability. Thus, the 1 Hz data contain unwanted signals, including noise and surface wave signals, that must be minimized before it can be used for submesoscale analysis.

One approach to minimize these unwanted signals is to apply time-averaging to the data. To determine an appropriate averaging window that provides high-resolution and quality data, we applied progressive averaging and tested different methods to find a consistent cutoff. We examined velocity spectra, velocity difference variability, and structure functions to identify the optimal averaging window. The resulting averaged datasets were then tested using the aforementioned

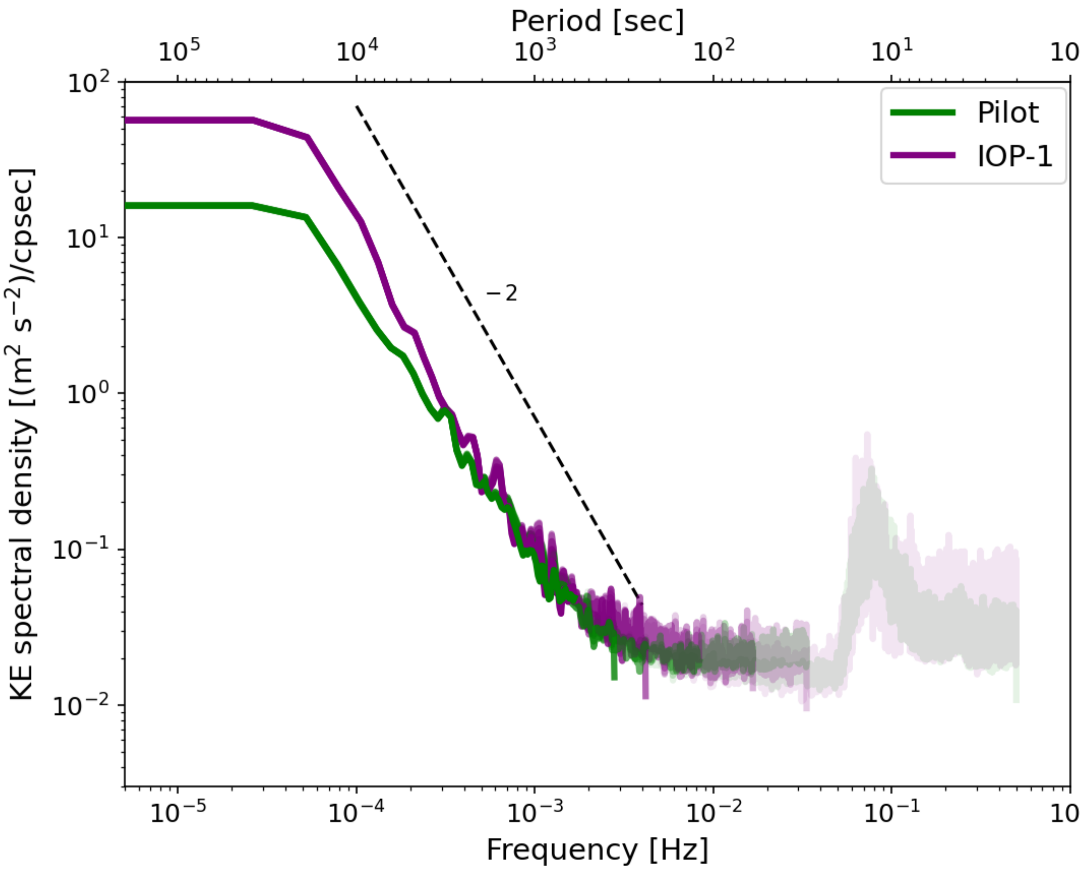

FIG. 4. Kinetic energy frequency spectra from two field campaign Saildrone ADCPs. The dashed line provides a reference -2 slope. Spectra of different averaging windows are shown in varying shading to illustrate the position of the Nyquist frequency, with shading progressing right to the left.

methods, allowing us to identify data with minimal unwanted signals and high temporal/spatial resolution. The KE spectra in Figure 4 demonstrate that with a 3-minute averaging window, unwanted signals are effectively minimized, leaving only submesoscale variability in the dataset with a power-law of approximately -2.

Figure 6 shows the velocity difference variability as a function of averaging window size. showing a decreasing trend with increasing averaging window before reaching a minimum at around 3 minutes. This suggests that a 3-minute average minimizes the variability due to noise and surface wave signals. This pattern of variability in velocity difference is observed in all four IOP-1 Saildrone datasets (figure not shown), with SD1048 showing higher error compared to the other three, due to one bad beam in SD1048 ADCP. Despite the higher error at 1 Hz, SD1048 follows the same decreasing trend and merges with the other Saildrone plots at a 3-minute averaging window.

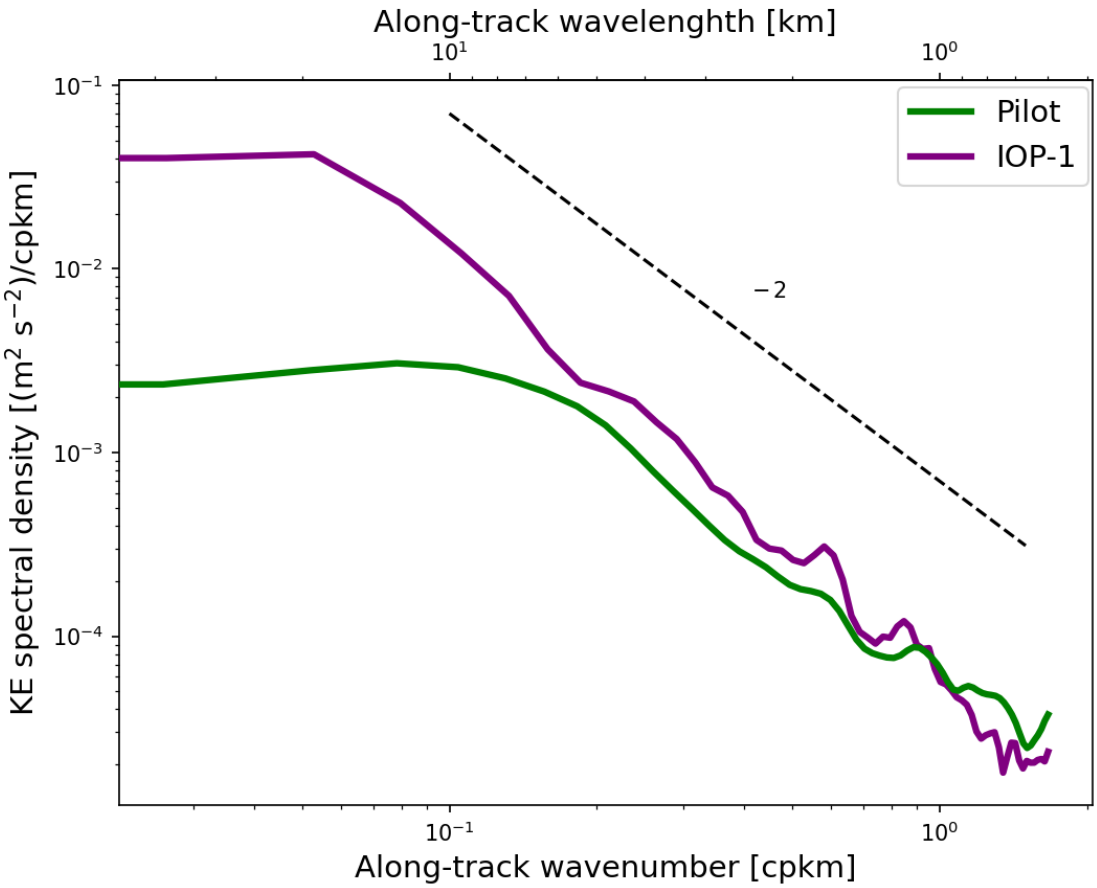

Fig. 5. Kinetic energy wavenumber spectra from two field campaign Saildrone ADCPs. The dashed line provides a reference -2 slope.

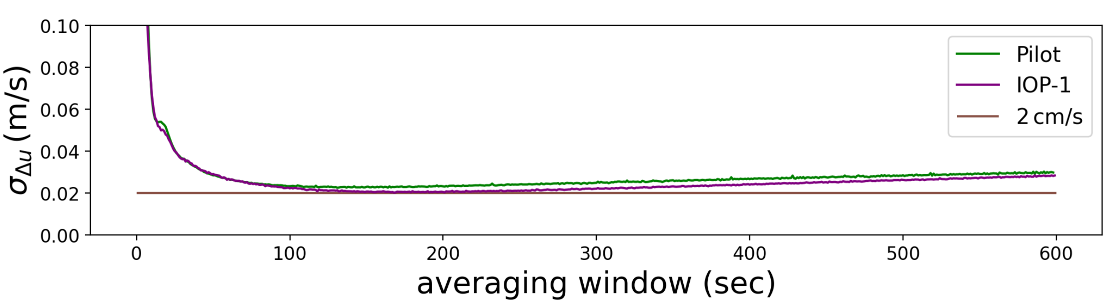

Fig. 6. Velocity difference variability across different averaging windows for both field campaign Saildrone ADCPs. The grey line represents 2 cm/s base.

We used the differential evolution function (Storn and Price 1997) to assess the minima in the velocity difference variability plots. In Figure 6, it is evident that the minimum values for the two Saildrones (SD1072 from the Pilot and SD1085 from IOP-1) are distinct yet closely positioned

(150s for the Pilot data and 188s for IOP-1). As a result, on average the 3-minute mark serves as the cut-off point for obtaining high-resolution, quality data for the Saildrones used in our experiments.

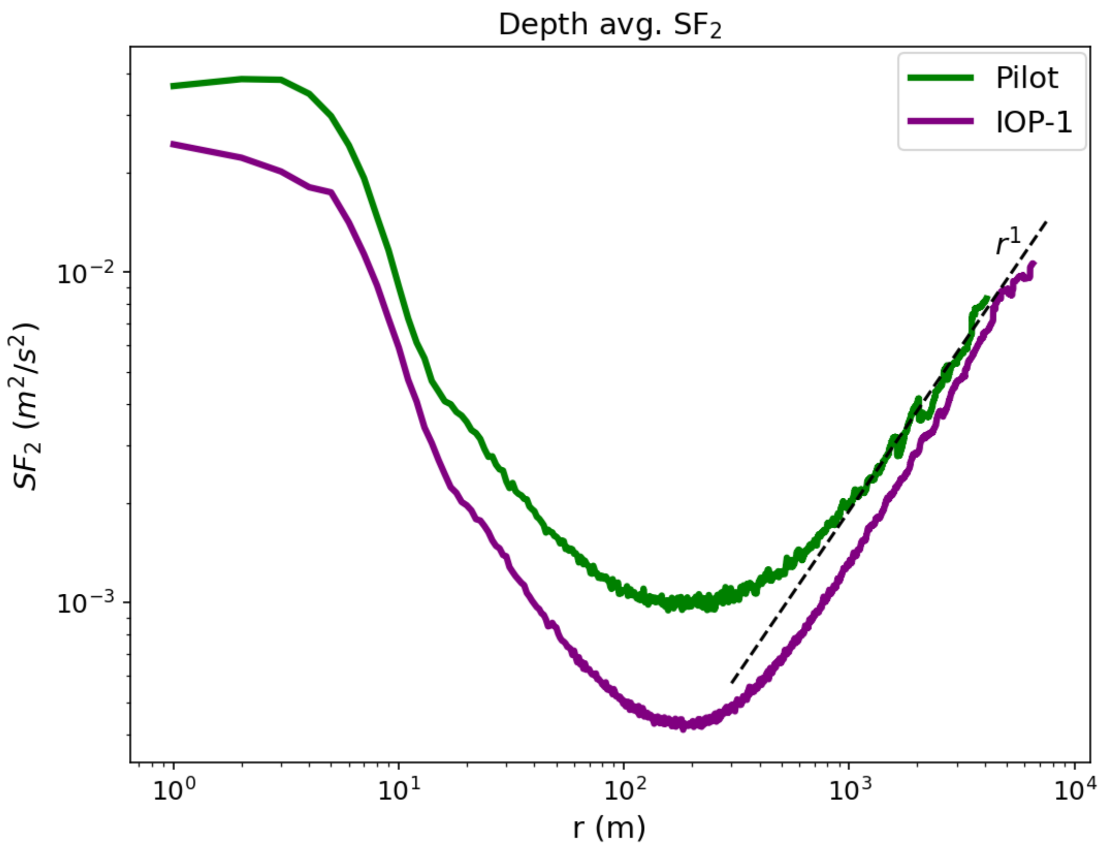

FIG. 7. Depth average structure-function of both field campaign Saildrone ADCPs. Dashed line provides a reference for the +1 slope.

The shortest time scale in which noise appears in the spectra and velocity difference variability analysis aligns with the associated spatial scales observed in the structure function (Figure 7). A similar result is obtained from the structure function analysis, where unwanted signals (noise and surface wave signals) decrease with increasing spatial averaging, consistent with the velocity difference variability analysis. The structure function in Figure 7 indicates a significant reduction in unwanted signals at a scale of approximately 250 meters, corresponding to the typical distance covered by a Saildrone in nearly 3 minutes. The observed +1 slope in the structure function corresponds to submesoscale variability, consistent with the -2 slope in the KE wavenumber spectra (Figure 5). Again, the differential evolution function (Storn and Price 1997) is applied to identify the minima in the SF (Figure 7). This function suggests that the minimum spatial averaging required for the Pilot and IOP-1 Saildrone data, as depicted in Figure 7, are 227 m and 205 m, respectively. Based on these findings, a 250-meter (3-minute) scale serves as the threshold for obtaining high-resolution data with high signal-to-noise ratio.

c. Depth-wise analysis

The structure function computed at all depths (< 50 m) shown in Figure 8 is obtained from the same data used in the analysis shown in Figure 7. The variability in Figure 8 is larger at small scales near the surface, in particular during the Pilot than IOP-1, when the significant wave height (H_s) approached 9 m, compared to IOP-1 with a maximum H_s of 4.5 m. Thus, we observe that the structure function minima occur at a scale that is 10 m larger for the Pilot compared to IOP-1 within the top 15 m depth. This indicates the need for a wider averaging window to reduce noise/surface wave signals near the surface during high wave conditions, as opposed to deeper depths. However, for consistency, we prefer to apply the same averaging window to the entire water column, for example, when computing horizontal velocity gradients or vertical velocity at the same spatial location but different depths. All three methods described in section 4b, aided by depth-wise

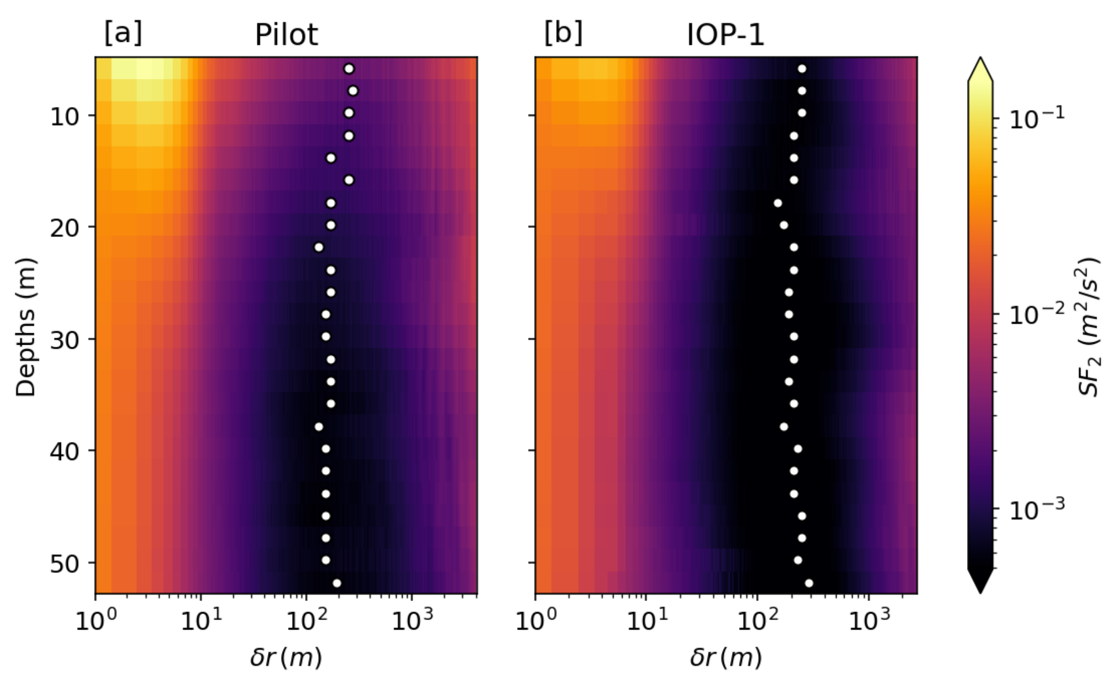

FIG. 8. Depth wise structure-function for the Pilot field campaign [a], and IOP-1 [b] Saildrone ADCP data. White dots indicate the minima in the structure function at each depth. This figure highlights the optimal averaging window required at each depth to achieve minimum noise and high-resolution data.

analysis above, are consistent in showing that 3-minute ($\sim$ 250 m) averaging provides the highest resolution while minimizing the presence of unwanted signals for submesoscale observations.

d. Velocity gradient uncertainties

Observing submesoscale processes is challenging because these are small-scale and short-lived, evolving much faster than the mesoscale features that oceanographers have traditionally sampled. Moreover, finding and tracking submesoscale features requires wide and dense sampling, making it a laborious task. The S-MODE experiments using several Saildrones with specific formations provide an excellent dataset for studying the sensitivity of submesoscale velocity gradient quantities, such as vorticity, divergence, and strain rate to the sampling pattern, which can also inform about the errors involved in these measurements. Despite the environmental challenges of sustaining Saildrones in formation, we sampled four times across a strong oceanic front in 36 hours with the 4 Saildrones maintaining the desired quad formation (Figure 9).

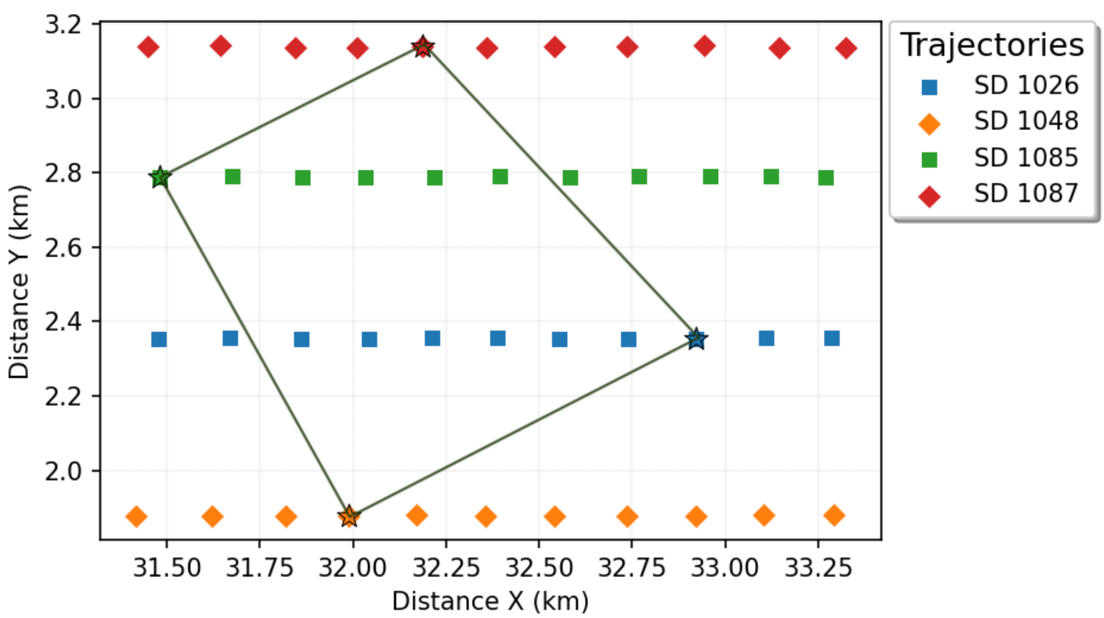

Fig. 9. Example of a single 2 km by 2 km box used in the computation of submesoscale velocity gradients, highlighting the quad formation piloting. The aliased 4 Saildrone velocity gradient calculation, using data from all points within the box, has an RMS average scale of ~750 m. The aliased 2 Saildrone calculation, using only data from the outer Saildrones (diamond dots), has an RMS average scale of ~850 m. The unaliased calculation, using data from the dots in the quad (marked by stars), has an RMS average scale of ~1 km.

For analysis in this subsection, data from only one leg out of the four is used for detailed comparison. This allows us to show the magnitude and variability of the errors more clearly. As the maximum across-track spacing of the quad formation reached to nearly 2 km at times, we search the data in a sliding box of 2 km by 2 km centered on the mean track of 4 Saildrones. We intend to examine the impact of using the frozen field approximation, a form of aliasing, on submesoscale velocity gradients, and the finest resolution of data attainable by Saildrone for submesoscale analysis.

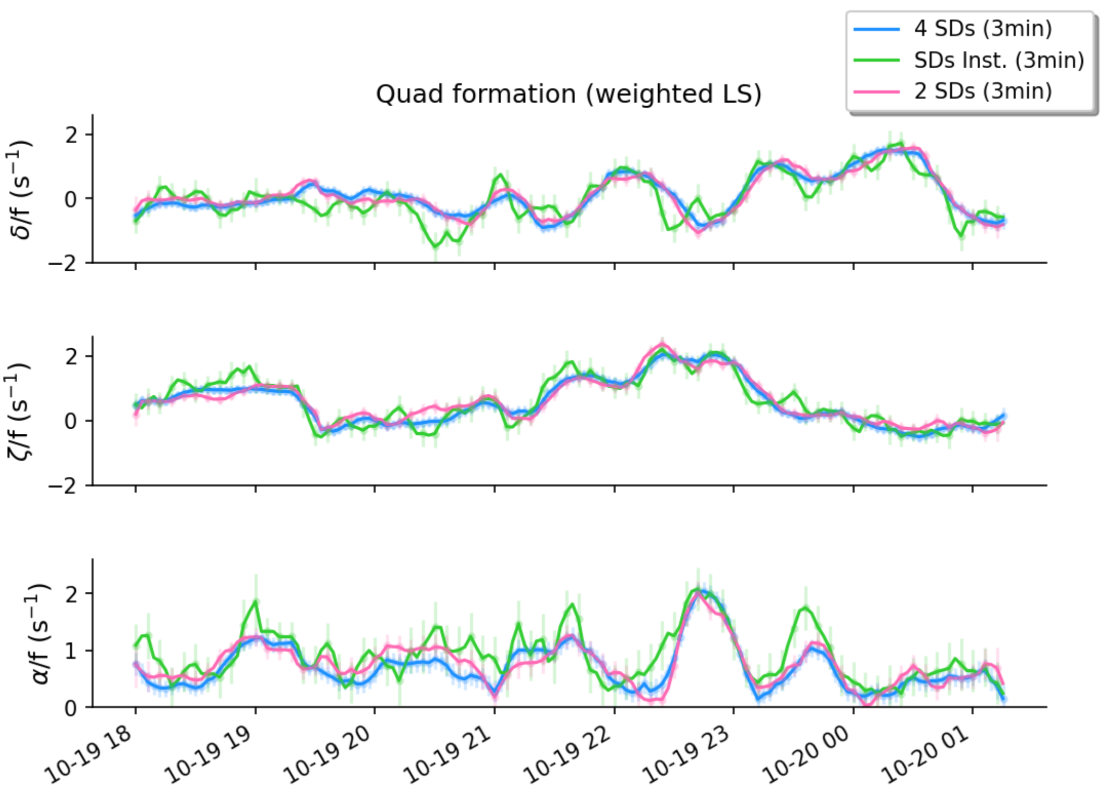

FIG. 10. Comparison of aliased and unaliased normalized-divergence (top), -vorticity, (middle) and -strain rate (bottom). The unaliased (Instantaneous) values (in green) are computed from 4 SDs instantaneously and averaged over a 2 km by 2 km box at 6 m depth. The alised values are computed from all the points in a 2 km by 2 km box, using all the 4 Saildrones (dodger blue) or only 2 farthest Saildrones in the formation (pink). The vertical lines represent 95% confidence level.

We assess the impact of aliasing on the velocity gradient calculations at 2 km scale (Figure 10) using the 3-minute data. This involves comparing the average unaliased-velocity gradients within the 2 km by 2 km box (Figure 9) to the aliased calculations for the same box using data from 2 and 4 Saildrones (Figure 10). The chosen track maintained a linearity of 0.6 (Figure 9) allowing for a direct comparison. The signals from all three approaches shown in Figure 10 are comparable and generally within error bars, which suggests that aliasing minimally impacts the accuracy of velocity gradient calculation at this scale. The unaliased results (from 4 Saildrones) for vorticity and divergence are comparable to the aliased results obtained using 2 Saildrones. However, unaliased estimate of the strain rate is significantly larger at times. This could be attributed to aliasing effect, differences in a scales, or number of data points.

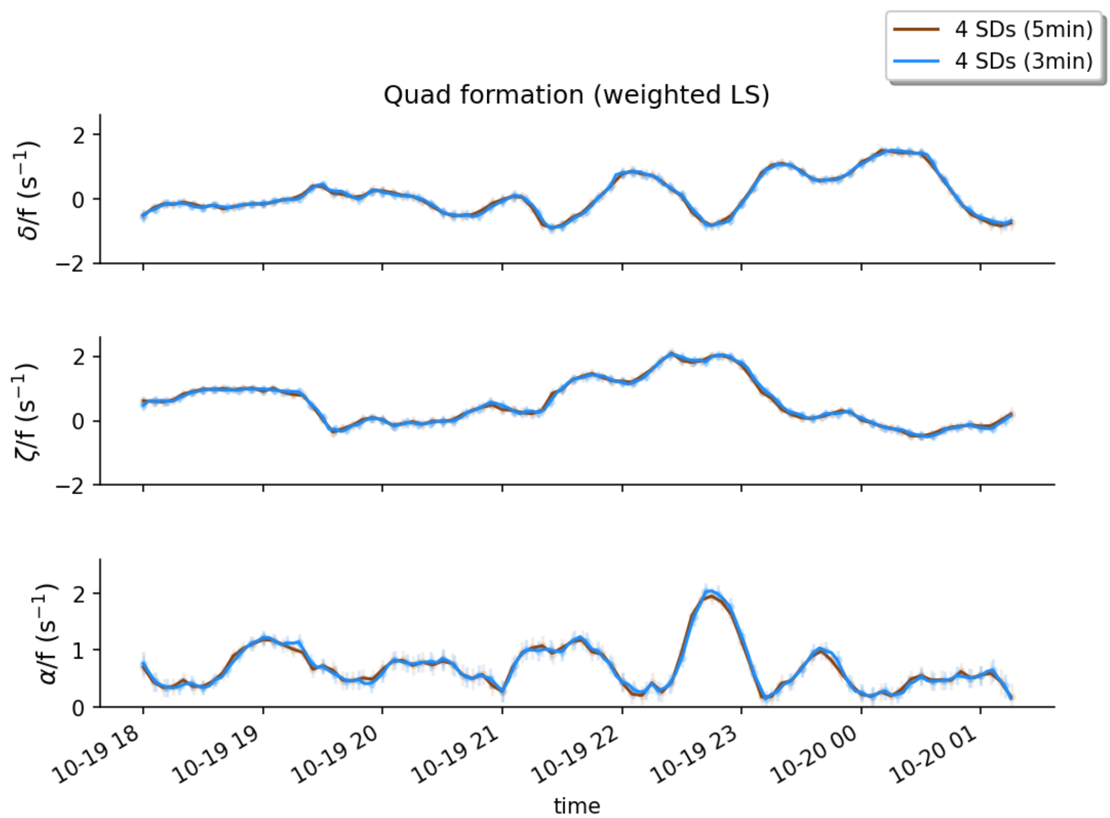

FIG. 11. Comparison of 5-minute vs 3-minute Weighted LS normalized-divergence (top), -vorticity (middle), and -strain rate (bottom) derived from Saildrones in quad formation data at a depth of 6 m. The vertical lines indicates the 95% confidence level.

Notice that the uncertainty and variability of the vorticity, divergence, and straining rate are larger for the unaliased data, which is because the unaliased data has fewer samples and a more limited spatial distribution. On average, there are 3 unaliased estimates from 4 Saildrones that are combined together (total of 12 data points) compared to 40 aliased data points from 4 Saildrones and 20 from 2 Saildrones (Figure 9). This suggest that averaging the unaliased calculations from four Saildrones over a 2 km by 2 km box can be deemed reliable.

Finally, we compare the standard 5-minute average ADCP for the computation of the current gradients. As expected, we show in Figure 11 that the velocity gradients estimated with the 3-minute data are consistent with those calculated with the 5-minute data, computed within the same 2 km by 2 km boxes. Thus, to take advantage of the finer resolution offered by 3-minute data, a tighter formation of the Saildrones would be required to obtain higher resolution gradients.

5. Summary

The prospect of observing the velocity field and its gradients from arrays of uncrewed surface vehicles (USVs) is very attractive, but it is important to characterize the quality of the ADCP data from USVs to understand the extent to which these gradient estimates can be trusted. This study compared synchronous ADCP measurements from Saildrones with those from the R/V *Oceanus* collected during the S-MODE field campaigns. The along-track velocity difference variability of Saildrone ADCP matches that with 3 cm/s of R/V *Oceanus* data, supporting its suitability for submesoscale studies. We also investigated the choice of averaging interval for velocity data to minimize noise and the unwanted wave signals using three different methods (sections 3c, 3d, 3e) that can also be applied to other surface vehicles. This investigation indicated that a 3-minute (or ~250 m) averaging of the Saildrone data provides high-quality, high-resolution information. We recommend employing any of the three methods along with the differential evolution function to determine the optimal averaging window. We then used this 3-minute data to determine the uncertainty in Saildrone velocity gradients and derived kinematic properties (vorticity, divergence, and strain rate) through the analysis of synchronous velocity measurements from Saildrones in formation.

The unaliased (instantaneous) velocity gradients obtained from 4 data points in the quad formation exhibit uncertainties with mean absolute value in the range $0.3f$–$0.6f$. To incorporate more data from these 4 Saildrones into the calculations of these velocity gradients, we used a 2 km by 2 km box approach. Both aliased and average unaliased calculations at this 2 km scale generally agree, except for few instances of strain rate. This suggest that either approach can be adopted, with uncertainties of $0.4f$ for the unaliased computation and $0.12f$ for the aliased computation. Further, testing with a case considering data from only the 2 outer Saildrone in the formation (a subset of the quad) indicates that the obtained aliased values at 2 km scale is comparable to the values obtained from 4 Saildrones, with uncertainties in the range of $0.25f$.

Acknowledgments. We thank the S-MODE Science Team for helpful discussions. Saildrone data were collected as part of the Submesoscale Ocean Dynamics Experiment, which is supported by the National Aeronautics and Space Administration (NASA Research Announcement NNH17ZDA001N-EVS3). The analysis of Saildrone data is being supported by the National Science Foundation (NSF award 2146729), São Paulo Research Foundation (FAPESP award 2023/10506-0) and Instituto Serrapilheira (SERRAPILHEIRA award 2211-41837).

Data availability statement. S-MODE Saildrone and R/V *Oceanus* data are freely available at https://podaac.jpl.nasa.gov/S-MODE.

APPENDIX

A1. Uncertainty in the coefficients of weighted least-squares plane fit

To estimate the uncertainties in the velocity gradients obtained from the weighted least-squares plane fit, we begin by scaling equation (5) with a weight matrix $\mathbf{W}^{-1/2}$, where $\mathbf{W} = \langle \mathbf{U}\mathbf{U}^{\mathrm{T}} \rangle$. Assuming the errors are uncorrelated, $\mathbf{W}$ is given by

$$\mathbf{W} = \begin{bmatrix} \epsilon_1^2 & 0 & 0 & \cdots & 0 \\ 0 & \epsilon_2^2 & 0 & \cdots & 0 \\ \vdots & 0 & \ddots & \cdots & \vdots \\ 0 & \vdots & 0 & \epsilon_{n-1}^2 & 0 \\ 0 & 0 & 0 & 0 & \epsilon_n^2 \end{bmatrix}, \tag{A1}$$

with ϵ_i the uncertainty (standard error) of i^{th} 3- or 5-minute averaged velocity observation (computed from the 1 Hz data). The weighted form of equation (5) is:

$$\mathbf{W}^{-1/2}\mathbf{U} = \mathbf{W}^{-1/2}\mathbf{X}\mathbf{A_u}. \tag{A2}$$

And the normal equation of the weighted least-squares case becomes:

$$\mathbf{X}^{\mathrm{T}}\mathbf{W}^{-1}\mathbf{X}\mathbf{A_u} = \mathbf{X}^{\mathrm{T}}\mathbf{W}^{-1}\mathbf{U}\,. \tag{A3}$$

Thus the least-squares solution for the model coefficients is:

$$\mathbf{A_u} = (\mathbf{X}^{\mathrm{T}}\mathbf{W}^{-1}\mathbf{X})^{-1}\mathbf{X}^{\mathrm{T}}\mathbf{W}^{-1}\mathbf{U}\,. \tag{A4}$$

The uncertainty in the model coefficients is derived by forming the covariance of $\mathbf{A_u}$:

$$\mathrm{Cov}(\mathbf{A_u}) = \langle \mathbf{A_u}\mathbf{A_u}^{\mathrm{T}} \rangle \tag{A5}$$

$$= (\mathbf{X}^{\mathrm{T}}\mathbf{W}^{-1}\mathbf{X})^{-1}\mathbf{X}^{\mathrm{T}}\mathbf{W}^{-1}\langle \mathbf{U}\mathbf{U}^{\mathrm{T}} \rangle \mathbf{W}^{-1}\mathbf{X}(\mathbf{X}^{\mathrm{T}}\mathbf{W}^{-1}\mathbf{X})^{\mathrm{T}-1} \tag{A6}$$

$$= (\mathbf{X}^{\mathrm{T}}\mathbf{W}^{-1}\mathbf{X})^{-1}\,. \tag{A7}$$

Assuming a Student's t-distribution, the 95% confidence intervals of $\mathbf{A_u}$ are given by twice the square root of the diagonal terms in $\mathrm{Cov}(\mathbf{A_u})$. Uncertainties in $\mathbf{A_v}$ are calculated analogously. This estimate of the velocity gradient uncertainties neglects the position inaccuracy stemming from the Saildrone's VN-300 IMU/GPS, which operates at 20 Hz. While this IMU/GPS has a velocity uncertainty of 5 cm/s (VN-300 manual) at 20 Hz, it translates to a velocity error of approximately 1 mm/s when data are averaged over a 5-minute span, rendering it negligible.

References

Alderson, S., and S. Cunningham, 1999: Velocity errors in acoustic doppler current profiler measurements due to platform attitude variations and their effect on volume transport estimates. *Journal of Atmospheric and Oceanic Technology*, **16 (1)**, 96–106.

Amador, A., S. Jaramillo, and G. Pawlak, 2017: ADCP bias and Stokes drift in AUV-based velocity measurements. *Journal of Atmospheric and Oceanic Technology*, **34 (9)**, 2029–2042.

Bennett, A., 1984: Relative dispersion: Local and nonlocal dynamics. *Journal of Atmospheric Sciences*, **41 (11)**, 1881–1886.

Callies, J., and R. Ferrari, 2013: Interpreting energy and tracer spectra of upper-ocean turbulence in the submesoscale range (1–200 km). *Journal of Physical Oceanography*, **43 (11)**, 2456–2474.

Capet, X., J. C. McWilliams, M. J. Molemaker, and A. F. Shchepetkin, 2008: Mesoscale to submesoscale transition in the california current system. part i: Flow structure, eddy flux, and observational tests. *Journal of physical oceanography*, **38 (1)**, 29–43.

Choi, J., A. Bracco, R. Barkan, A. F. Shchepetkin, J. C. McWilliams, and J. M. Molemaker, 2017: Submesoscale dynamics in the northern gulf of mexico. part iii: Lagrangian implications. *Journal of Physical Oceanography*, **47 (9)**, 2361–2376.

D'Asaro, E. A., and Coauthors, 2018: Ocean convergence and the dispersion of flotsam. *Proceedings of the National Academy of Sciences*, **115 (6)**, 1162–1167.

Essink, S., V. Hormann, L. R. Centurioni, and A. Mahadevan, 2019: Can we detect submesoscale motions in drifter pair dispersion? *Journal of Physical Oceanography*, **49 (9)**, 2237–2254.

Ferrari, R., and C. Wunsch, 2010: The distribution of eddy kinetic and potential energies in the global ocean. *Tellus A: Dynamic Meteorology and Oceanography*, **62 (2)**, 92–108.

Gentemann, C., and Coauthors, 2020: Saildrone: Adaptively sampling the marine environment. *Bulletin of the American Meteorological Society*, **101 (6)**, E744–E762.

Hodges, B. A., L. Grare, B. Greenwood, K. Matsuyoshi, N. Pizzo, N. M. Statom, J. T. Farrar, and L. Lenain, 2023: Evaluation of ocean currents observed from autonomous surface vehicles. *Journal of Atmospheric and Oceanic Technology*, **40 (10)**, 1121–1136.

Joyce, T. M., 1989: On in situ "calibration" of shipboard adcps. *Journal of Atmospheric and Oceanic Technology*, **6 (1)**, 169–172.

Kämpf, J., and P. Chapman, 2016: *Upwelling systems of the world*. Springer.

Kessouri, F., D. Bianchi, L. Renault, J. C. McWilliams, H. Frenzel, and C. A. Deutsch, 2020: Submesoscale currents modulate the seasonal cycle of nutrients and productivity in the california current system. *Global Biogeochemical Cycles*, **34 (10)**, e2020GB006 578.

Kosro, P. M., 1985: *SHIPBOARD ACOUSTIC CURRENT PROFILING DURING THE COASTAL OCEAN DYNAMICS EXPERIMENT (DOPPLER, ACOUSTICS, SHELF)*. University of California, San Diego.

Lévy, M., R. Ferrari, P. J. Franks, A. P. Martin, and P. Rivière, 2012: Bringing physics to life at the submesoscale. *Geophysical Research Letters*, **39 (14)**.

Mahadevan, A., and A. Tandon, 2006: An analysis of mechanisms for submesoscale vertical motion at ocean fronts. *Ocean Modelling*, **14 (3-4)**, 241–256.

Marchesiello, P., J. C. McWilliams, and A. Shchepetkin, 2003: Equilibrium structure and dynamics of the california current system. *Journal of physical Oceanography*, **33 (4)**, 753–783.

McWilliams, J. C., 2016: Submesoscale currents in the ocean. *Proceedings of the Royal Society A: Mathematical, Physical and Engineering Sciences*, **472 (2189)**, 20160 117.

Molinari, R., and A. Kirwan, 1975: Calculations of differential kinematic properties from lagrangian observations in the western caribbean sea. *Journal of Physical Oceanography*, **5 (3)**, 483–491.

Ohlmann, J., M. Molemaker, B. Baschek, B. Holt, G. Marmorino, and G. Smith, 2017: Drifter observations of submesoscale flow kinematics in the coastal ocean. *Geophysical Research Letters*, **44 (1)**, 330–337.

Okubo, A., and C. C. Ebbesmeyer, 1976: Determination of vorticity, divergence, and deformation rates from analysis of drogue observations. *Deep Sea Research and Oceanographic Abstracts*, Elsevier, Vol. 23, 349–352.

Poje, A. C., T. M. Özgökmen, D. J. Bogucki, and A. Kirwan, 2017: Evidence of a forward energy cascade and kolmogorov self-similarity in submesoscale ocean surface drifter observations. *Physics of Fluids*, **29 (2)**.

Press, W. H., 1992: Sa teukolsky, wt vetterling and bp flannery, numerical recipes in fortran. Cambridge university press.

Qu, L., and Coauthors, 2022: Rapid vertical exchange at fronts in the northern gulf of mexico. *Nature Communications*, **13 (1)**, 5624.

Rocha, C. B., S. T. Gille, T. K. Chereskin, and D. Menemenlis, 2016: Seasonality of submesoscale dynamics in the kuroshio extension. *Geophysical Research Letters*, **43 (21)**, 11–304.

Romero, L., and W. K. Melville, 2010: Airborne Observations of Fetch-Limited Waves in the Gulf of Tehuantepec. *Journal of Physical Oceanography*, **40 (3)**, 441–465, https://doi.org/10.1175/2009JPO4127.1.

Rudnick, D. L., 1996: Intensive surveys of the azores front: 2. inferring the geostrophic and vertical velocity fields. *Journal of Geophysical Research: Oceans*, **101 (C7)**, 16 291–16 303.

Rudnick, D. L., 2001: On the skewness of vorticity in the upper ocean. *Geophysical Research Letters*, **28 (10)**, 2045–2048.

Shcherbina, A. Y., E. A. D'Asaro, C. M. Lee, J. M. Klymak, M. J. Molemaker, and J. C. McWilliams, 2013: Statistics of vertical vorticity, divergence, and strain in a developed submesoscale turbulence field. *Geophysical Research Letters*, **40 (17)**, 4706–4711.

Storn, R., and K. Price, 1997: Differential evolution–a simple and efficient heuristic for global optimization over continuous spaces. *Journal of global optimization*, **11**, 341–359.

Su, Z., J. Wang, P. Klein, A. F. Thompson, and D. Menemenlis, 2018: Ocean submesoscales as a key component of the global heat budget. *Nature communications*, **9 (1)**, 1–8.

Teledyne, R. I., 2010: Adcp coordinate transformation: formulas and calculations. *TELEDYNE RD INSTRUMENTS, Technical manual*.

Zhang, D., and Coauthors, 2019: Comparing air-sea flux measurements from a new unmanned surface vehicle and proven platforms during the spurs-2 field campaign. *Oceanography*, **32 (2)**, 122–133.